Proceedings of the 23rd International Congress on Applications of Lasers and Electro-Optics 2004

RESPONSE OF THIN FILMS AND SUBSTRATE TO MICRO SCALE LASER SHOCK PEENING

Youneng Wang, Hongqiang Chen, Jeffrey W. Kysar, Y. Lawrence Yao

Department of Mechanical Engineering
Columbia University, New York, NY 10027

Abstract

Micro scale laser shock peening (μLSP) can potentially be applied to metallic structures in micro devices to improve fatigue and reliability performance. Copper thin films on single-crystal silicon substrate are treated by using μLSP and characterized using techniques of X-ray micro-diffraction and electron backscatter diffraction (EBSD). Strain field, dislocation density and microstructure changes including crystallographic texture, grain size and subgrain structure are determined and analyzed. Further, shock peened single crystal silicon was experimentally characterized to better understand its effects on thin films response to μLSP. The experimental result is favorably compared with FEM simulation based on single crystal plasticity.

Introduction

The reliability and failure of micro-electromechanical system (MEMS) are of concerns for long-term applications and efforts have made on these aspects over the last few years [1]. MEMS devices like switchers and gears experience cyclic loads in applications, and actuators fail because of wear and friction of the rubbing surface. Silicon is the most dominant material in MEMS devices, but metals such as aluminium, copper, gold and nickel are often used in MEMS as electrical conductors and occasionally as structural material due to high electric conductivity and easier to work with than silicon. While metals are used, they are usually deposited as a film over a substrate, which is usually single crystal silicon. Consequently, improvement of reliability and fatigue performance of metallic thin film has been the subject of much research.

Microscale laser shock peening (μLSP) is a technique in which LSP is implemented using a laser beam of micron size. It can potentially be applied to manipulate the residual stress distribution in surface layers of metal structures with micron-level spatial resolution and thus enhance fatigue and reliability performances of micro-devices [2]. It was found by using X-ray micro-diffraction measurements that the micron sized beam still imparts appreciable compressive residual stress within bulk metals. Also, the response to μLSP for single crystal metals was numerically predicted by FEM analysis [2].

However, it is more desirable to understand the response of metallic thin films to μLSP since most of metal MEMS structures are made from metallic thin films. Zhang, et al. [3, 4] investigated the μLSP effects on copper thin film on silicon substrate through average stress and hardness evaluation. It was seen from the average stress measurement that compressive residual stress was induced into thin films by μLSP similar to bulk metals but with a reduced magnitude. Though the work of [3, 4] gives some insights into the area, it is far from completely understanding since there is no direct investigation about μLSP induced microstructural changes, such as crystallographic texture, grain and subgrain structures, which mechanical properties of thin film are highly dependent on. Therefore, it is of great interest to quantitatively characterize and understand microstructure changes after μLSP. Also, response of thin films to μLSP is more or less affected by substrate on which they are deposited. Metallic micro components are normally made by patterning metallic films on substrate and then sacrificing the substrate. Since μLSP needs to be applied between the two steps, it is definitely important to understand substrate response to μLSP in order to fully understand effects of μLSP to thin film on substrate.

In this paper, the copper thin films by μLSP was experimentally analyzed by both X-ray micro-diffraction and EBSD. In addition, silicon substrate after μLSP was investigated by X-ray micro-diffraction and FEM simulation. These investigations provide groundwork for further numerical and theoretical analysis of response of thin films with silicon substrate to μLSP.

Experiment Conditions

A frequency tripled Q-switched Nd:YAG laser in TEM_{00} mode with the parameters of pulse duration = 50ns, wavelength =355nm and beam diameter =12μm are used. Spacing between consecutive pulses along a shock line was 25μm and pulse repetition rate was 1KHz. Pulse energies, 356 and 228μJ, corresponding to laser intensities of 6.30 and 4.03GW/cm^2, respectively, were used. Detail information about μLSP refers to [2].

The samples are copper thin films of 1μm and 3μm thickness on (004) single crystal silicon wafer. The 1μm samples were prepared by physical vapor deposition (PVD) while the 3μm samples were by electroplating process. It can be seen from x-ray diffraction result as shown in Fig. 1 that both 1μm and 3μm samples show strong (111) texture. In addition, silicon wafers with (004) orientation were used for shocking experiments as well. For Si samples, the shocked line is carefully aligned with the [110] direction. In this way, the active slip systems are confined within the (110) plane and only plane and symmetric deformation is resulted [2].

Measurement and Characterization Methods

X-ray Microdiffraction Measurement

X-ray microdiffraction is a relatively new method in material characterization in micron scale resolution, which is required to characterize the samples treated by μLSP since the shocked area is usually in tens of microns [2]. In this case, high brightness synchrotron radiation sources are used for speed and accuracy in X-ray microdiffraction experiments at the beamline X20A of National Synchrotron Light Source (NSLS) in Brookhaven National Lab. The radiation energies for films and substrate are 8.0KeV and 8.5KeV, respectively, because copper films are less absorbent for the incident X-ray of 8.5KeV [5].

In the experiment, multiple points across the shock line were chosen for measurement. Because the surface at each point of film samples is not ideally parallel to each other and the incident x-ray beam is divergent, the x-ray incident should be realigned at each measurement position to satisfy Bragg angle condition. Here, χ and θ are optimized by scanning the diffracted intensity as a function of χ and θ respectively at each measurement location as shown in Fig. 2. Once the specimen tilt is properly set, the 2θ value of the peak can be measured by a detector scan in 2θ or by a radial scan where 2θ and θ are stepped at the symmetric 2:1 ratio. Also, in order to achieve the micron scale resolution, the x-ray incident spot size on the target should be as small as possible, which is related to divergent angle and distance from tip to target as shown in Fig. 2.

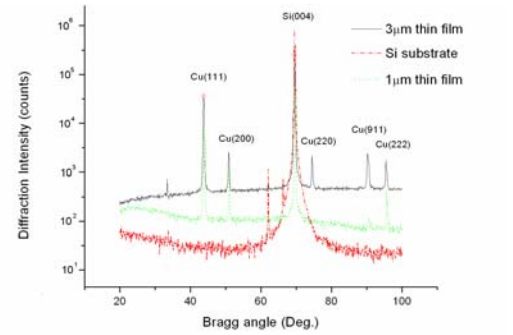

Fig. 1 Characterization of testing materials (1μm and 3μm Cu polycrystalline films on [004] single crystal Si substrate) by conventional X-ray diffraction

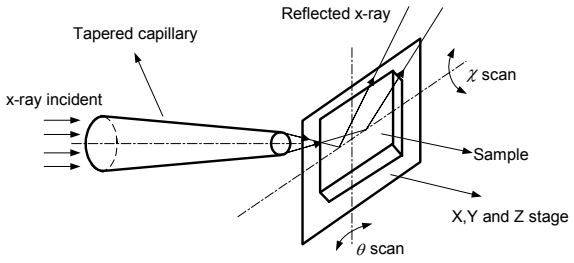

Fig. 2 Divergence of x-ray beam incident and θ, and χ scans of sample (distance from sample to the capillary tip is about 3mm, the focused spot size is about 2μm, the divergence angle is 0.6°, and the spot size on the sample surface is about 5μm)

X-ray Profile Evaluation Method By Fourier Transformation

The shock peening induces nonuniform strain and produces dislocation arrays, such as substructures or subgrains [2]. Both kinds of effects contribute to the broadening of the X-ray line profile in plastically deformed metals [6]. Based on the Fourier analysis of the diffraction profiles, the Warren & Averbach method [7] allows to obtain strain deviation and distribution function of grain size directly from the Fourier series coefficients.

From the analysis of [7], the sample can be represented as columns of unit cells along the direction which is perpendicular to the diffraction plane in the reciprocal lattice space. The X-ray line profile can be considered as the combination of reflected X-ray from all pairs of unit cells. The measured X-ray line profile is then represented as the Fourier series in the reciprocal lattice space [7]

$$P(2\theta) = \frac{KNF^2}{\sin^2\theta} \sum_{n=-\infty}^{+\infty} (A_n \cos 2\pi nh + B_n \sin 2\pi nh) \quad (1)$$

where $P(2\theta)$ represents the measured X-ray line profile *vs* 2θ, F is the structure factor and K is the angular factor, N represents the number of unit cells in the sample and h is the reciprocal of the lattice spacing. The real part of Fourier coefficient A_n can be described as the product of the size effect and the strain effect $A_n = A_n^S A_n^D$ [7]. Where A_n^D represents the spacing change between the diffraction planes and A_n^S is a measure of the grain size. Furthermore, for small values of l and n, A_n can be expressed by [7]:

$$\ln A_n = \ln A_n^S - 2\pi^2 l^2 n^2 < \varepsilon^2 > \quad (2)$$

where l is the number of unit cells between diffraction planes and $< \varepsilon^2 >^{1/2}$ is standard strain deviation which indicates strain uncertainty. According to Eqn. (2), $\ln(A_n)$ vs n^2 is represented as a straight line, whose slope and intersection with n = 0 can be used to evaluate the strain deviation and size effects.

According to [6], the analysis of Fourier coefficients of X-ray profiles shows that taking into account the dislocation effect on the profiles gives a modified method, known as the modified W-A analysis. This procedure enables a straightforward determination of dislocation density from X-ray line profile analysis. For crystals containing dislocations, the diffraction profile is also considered as the combination of the diffracted X-ray for all unit cells in crystal as that in Warren's method. However, the displacement of each unit cell is represented by the dislocation Burgers vector to account for the effect of dislocation structure and the real part of the Fourier coefficients of the X-ray line profile can be written as [6]

$$\ln A_n = c_0 - \rho^* n^2 \ln(R_e / n) + Q^* n^4 \ln(R_2 / n) \ln(R_3 / n) \quad (3)$$

where ρ^* is the "formal" dislocation density, directly available from a broadened profile without taking into account the effect caused by different types of dislocations. Q^* is given as the variation of the dislocation density, n is the harmonic number, and R_e is the outer cutoff radius of dislocations, which indicates the distribution range of dislocation stored energy. R_2 and R_3 are auxiliary constants. The true value of dislocation density is $\rho = \frac{2\rho^*}{\pi g^2 b^2 \overline{C}}$. Where $\overline{C}$ is the average contrast factor for different type of dislocations (edge and screw) in the case of a particular *hkl* reflection and can be found in [6], b is the Burgers vector of dislocations which is *a/2*<110> here for *FCC* metals and g is the diffraction vector. Thus, after calculating the real part of the Fourier coefficients A_n, the $\ln(A_n)$~n data can be fitted as a non-linear curve using formula in Eqn. (3). The parameters such as ρ^* can be determined in curve fitting using least-squares evaluation method and the dislocation density ρ can be evaluated.

EBSD Measurement

EBSD is used to examine a wide range of crystalline materials and to measure microstructure, orientation, texture and boundary properties. In this paper, microstucture including texture, grain and subgrain structures was studied for 1μm film samples. CHANNEL5 EBSD system of HKL Technology was employed, which is attached to a JEOL JSM 5600LV scanning electron microscope. The shocked area was accurately located using SEM before EBSD measurement by marking the shock line in several points during shock peening with three more pulses.

Results and Discussion

Characterization Of Shocked Thin Films Via X-ray Microdiffraction Analysis

Strain deviation, grain size and dislocation density In order to better understand shock-induced plastic deformation, it is necessary to study the corresponding inhomogeneous strain variation in the depth direction, which can be calculated from the recorded X-ray profiles (Fig. 3) according to the method discussed in Section 3.2. From the theory of [7], for small values of l and n, the logarithm of the measured Fourier coefficient is given by Eqn. (2). For (111) reflection, l=3, so the strain effect term can be represented as $-2\pi^2 l^2 n^2 < \varepsilon_l^2 >$, in which $< \varepsilon_l^2 >^{1/2}$ represented standard strain deviation caused by the laser shock peening in the <111> direction. If we choose n^2 as the X-axis and $lnA_n(l)$ as the Y-axis, Eqn. (2) represents a straight line with slope $K = -2\pi^2 l^2 < \varepsilon^2 >$. Thus, the slope of this fitted line can be used to calculate the strain deviation $< \varepsilon_l^2 >^{1/2} = \sqrt{\frac{K}{-2\pi^2 l^2}}$. X-ray profiles at each position cross the shocked line, from 40μm left of the shocked line to 40μm right, were processed by using Fourier transformation with Stoke's correction [8] based on lnA_n vs n^2 lines as shown in Fig. 4. Fig. 5 shows the result of the spatial distribution of strain deviation in depth direction. It can be seen that the maximum deviation is about ±0.025 at the center and decreases to zero at around ±30μm from the center, which strongly indicates that non-uniform strain is induced by laser shock peening.

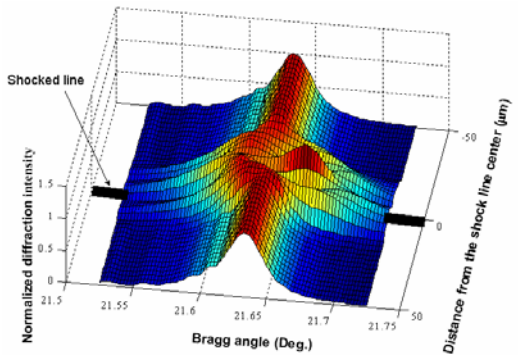

Fig.3 3D X-ray profile spatial distribution across the shock line of 3μm thin film (laser energy of 6.30 GW/cm^2, spatial resolution is 5μm close to the line and 10μm far away from the line)

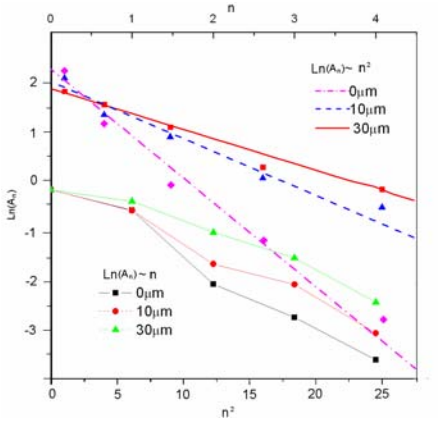

Fig. 4 Ln(A_n) vs n^2 and Ln(A_n) vs n lines at different positions from the center of shocked line (A_n: the real part of corrected Fourier coefficient; and n: Fourier series number)

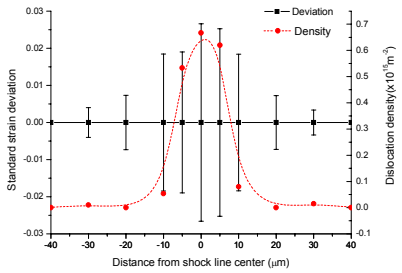

Fig. 5 Standard strain deviation in depth direction and dislocation density by Fourier transformation for the 3μm copper thin film

Dislocation cell structures were observed via TEM in laser shock penned metals such as Copper. This accompanies the generation and storage of a higher dislocation density than that from quasi-static deformation processes. It is of interest to study the magnitude and spatial distribution of dislocation density under μLSP. Within the formalisms of the kinematical scattering of X-rays and the linear elasticity theory of dislocations, modified Warren-Averbach method was used to evaluate the dislocation density from the X-ray profile analysis [6]. According to Eqn. (3), non-linear curve fitting with the least-squares evaluation was applied to the plot of the Fourier coefficients ln(A_n) vs n (Fig. 4). All six parameters c_0, ρ^*, Q^*, R_e, R_2, and R_3 were calculated through six curve fitting parameters $P1$ to $P6$. After obtaining the formal dislocation density ρ^*, the true values of dislocation density is calculated. Fig. 5 shows the dislocation density across the shock line. As seen, the highest density occurs at the shock line center and decays slowly to the outer edge. The result is again consistent with the strain deviation result.

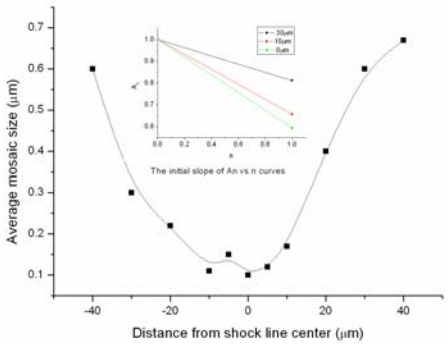

Fig. 6 Spatial distribution of average mosaic size by FFT analysis of the initial slopes of the A_n vs. n curves (as shown in the small figure) for 3μm copper film

As discussed before, size broadening effect is represented by a cosine Fourier series similar to that developed for strain broadening and hence the Fourier coefficients A_n give very general method of handling either effect. From the analysis of [7], the initial slope of the A_n vs n curve is $(\frac{dA_n}{dn})_{(n=0)} = -\frac{1}{\overline{N}_3}$, where $\overline{N}_3 a_3$ is the average column length and hence an average grain size in the direction a_3. So if the size broadening effect is expressed in terms of a plot of the Fourier coefficients A_n vs n, the initial slope of the curve gives directly the average column length, which is the average grain size in that direction.. If the initial slope of curve is K, then the average grain size D at that position can be evaluated as $D = (1/K) \cdot a_3$. From the analysis above, the size effect can be obtained from Fourier analysis of X-ray profiles. Fig. 6 shows the spatial distribution of average grain size evaluated from the X-ray profile analysis mention above. It can be seen that the average grain size decreases when move closer to the shock line center. In the region of ±20μm from the center, the

grain size is around 0.1μm to 0.2μm. Therefore, the shocked area is strengthened due to a mosaic size refinement, according to well-known empirical relationship such as the Hall-Petch relation.

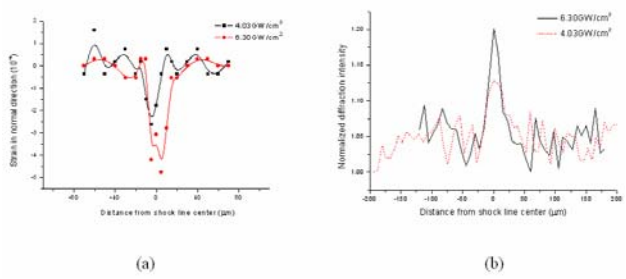

Fig. 7 X-ray diffraction measurements for (004) single crystal silicon: a) spatial distribution of strain normal to the irradiated surface; b) intensity contrast

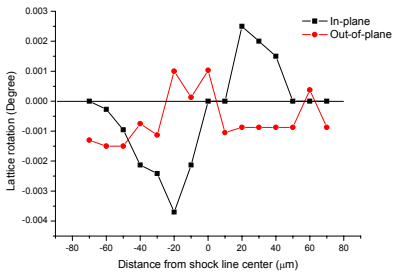

Fig. 8 In-plane and out-of-plane lattice rotation on shock peened surface of single crystal silicon for 4.03GW/cm^2 laser energy (obtained from the θ and χ scans, respectively, shown in Fig. 2)

Characterization Of Silicon Substrate Via X-ray Microdiffraction Analysis

For the substrate silicon, the shocked line is along the [110] direction, which results in a predominately plane deformation state in (110) plane. This was shown in [2] and will be discussed in the simulation section in more detail. It was found that x-ray profile for silicon (004) after μLSP is shifted to higher angle and there is almost no broadening, that is, μLSP results in almost uniform and elastic strain in normal direction of the substrate. By using Bragg law $\Delta d/d = -\cot\theta\,\Delta\theta$, the strain distribution in normal direction is obtained and shown in Fig. 7a. It can be seen that the effected region of μLSP for the substrate is about ±20μm and the same as that for thin film at both laser energy levels. Also, it is consistent with the result by diffraction intensity contrast, which is shown in Fig. 7b. Fig. 7a shows that the maximum strain in normal direction induced by μLSP is below 0.05%, which means that μLSP with these two laser energy levels has little effect on the silicon substrate.

As mentioned in Section 3.1, two rotations, θ scan and χ scan were applied in the X-ray diffraction experiment to minimize divergence effect (Fig. 2). The θ scan ensures that the mean beam vector of incident X-ray is at the proper angle with respect to the surface. The χ scan ensures that the normal vector of the diffracting plane is contained in the same geometrical plane as the incoming and diffracted X-ray beams. These two scans applied iteratively optimize the integrated intensity of the relevant reflection during alignment. Therefore, the in-plane and out-plane lattice rotation can be obtained from the θ and χ scans respectively. From Fig. 8, it is clear that the spatial distribution of in-plane lattice rotation in the substrate (004) is anti-symmetric with respect to the center of shock line. The maximum rotation angle is around ±0.003° at position nearly ±20μm away from the center of shock line. While the variation of out-of-plane lattice rotation in Fig. 8 is only ±0.001° and quite small relative to in-plane lattice rotation. The lattice rotation measurements confirm that the deformation is predominantly plane and symmetric about the shocked line center.

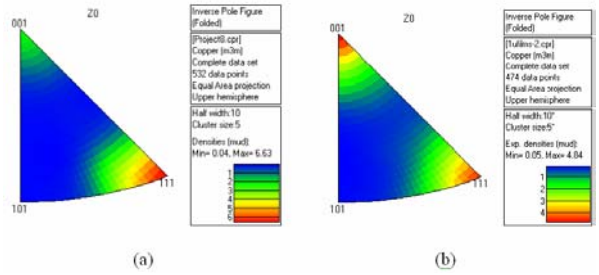

Fig. 9 Texture of 1μm thin film by inverse pole figure: a) raw sample; b) shocked area

Microstructure Characterization By EBSD

Crystallographic texture The physical properties of many samples are dependent on the common alignment of particular crystallographic directions: one of the easiest ways to view this is to use pole figures or inverse pole figures via EBSD. In order to determine the texture precisely, the scanning area is set as large as possible, i.e., 20μm×20μm since the effected width is about 25μm according to the X-ray microdiffraction results, and step size of 0.5μm was employed. From inverse pole figure of the unshocked 1μm film as shown in Fig. 9(a), it is clear that there is very strong (111) texture and relatively weak (001) texture, which is in accordance with the result of conventional x-ray diffraction. After μLSP, the corresponding inverse pole figure is shown in Fig. 9(b). It can be found that the (111) texture intensity is weakened, while (001)

texture intensity is enhanced. This change can be quantitatively analyzed through misorientation angle distribution of <001> direction, which is relative to the surface normal of the sample. Intensities close to zero degree is corresponding to density of (001) texture while intensities around 54.7° is for (111) texture. It can be seen that the maximum intensity at low angles is doubled after LSP while the intensities around angle 54.7° somewhat decrease.

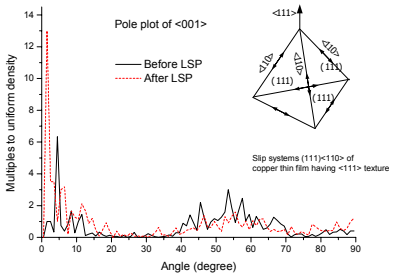

Fig. 10 Misorientation angle distribution of {001} lattice direction before and after LSP for 1μm thin film and slip systems (111)<110> for (111) film texture

The change from the (111) deformation texture to the (001) recrystallization texture could be explained by using the strain energy release maximization (SERM) model [9]. If a small volume of a uniaxially stressed body with fixed ends is replaced by the same volume of unstressed body, the strain energy of the system including the substituted region will be reduced. The released energy depends on Young's modulus of the substituted body and will be maximized if Young's modulus of the substituted body is minimum. Since copper is a *FCC* metal, and for this case slip systems for the copper thin film has the (111) orientation shown in Fig. 10. According to Schmid's law, total six slip systems except that with the plane (111) paralleling the film surface, which Schmid's factors are equal to zero, are activated when applying microscale LSP. The vector sum of the three indicated <110> directions becomes the <111> axis direction because of symmetry about indicated <111> direction [9]. Therefore, the <111> axis direction is the absolute maximum internal stress direction, which will become parallel to the minimum elastic modulus direction of recrystallized crystals according to the SERM model to maximize the released energy resulted from μLSP. For the copper, Young's modulus are 66.7 GPa in <100> direction, 191.1 GPa in <111> direction and 130 GPa in <110> direction. The minimum elastic modulus direction of copper thin film is the <100> direction. Therefore, the plastically deformed film having the (111) texture will have the (001) texture after recrystallization, which is in agreement with the measured results.

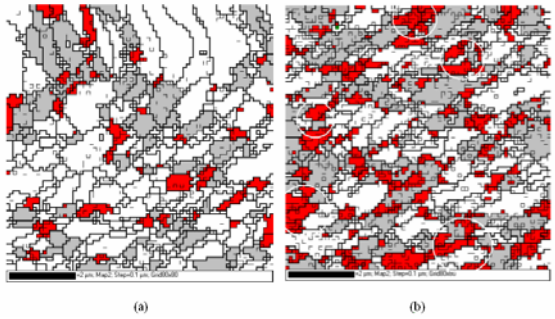

Fig. 11 Grain size map and subgrain structure changes through LSP of 1μm film: a) before LSP; b) after LSP. (Red color: highly deformed region with the highest density of substructure, Grey color: grains with medium density of substructures, White color: stress free grains that have less defects and substructures (Circles shown in b) are to be used with Fig. 14)

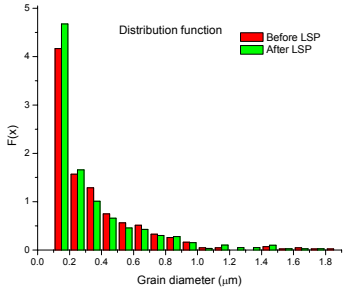

Fig. 12 Distribution of grain size for 1μm thin film

Grain size and subgrain structures Grain boundaries were distinguished by defining the corresponding misorientation angles and the grain size distribution of the sample were found using the EBSD post processing software. In this case, the misorientation angle of grain boundary is set to be 10 degrees, which is suitable for most of materials. Because the grain diameter is likely in the order of film thickness, the scanning area of 8μm×8μm and step size of 0.1μm were used. The maps of grain size before and after μLSP are shown in Fig. 11, in which the thick lines are the grain boundaries. By comparing Fig. 11(a) and (b), it is clear that after LSP the grain size becomes smaller and somewhat more uniform. The statistic results of Fig. 11 for distribution function of grain diameter as shown in Fig. 12 confirm that. This result is also in accordance with the result from atomic force microscopy (AFM) as shown in Fig. 13. Before LSP, the average diameter of grains is about 0.372μm and the standard deviation is 0.375; after LSP, the average diameter of grains is about 0.302μm and the standard deviation is 0.311. As a result of the grain size refinement, the shocked area is strengthened according to well-known empirical relationship such as the Hall-

Petch relation. Also, the more uniform distribution of grain size results in higher yield strength compared with the material with a more scattered grain size distribution. The reason is that plastic strain is unevenly distributed among grains of different sizes [10]. Uniform grain size tends to share the external load more uniformly and is desirable for neutralizing weak spots and thus stress concentration.

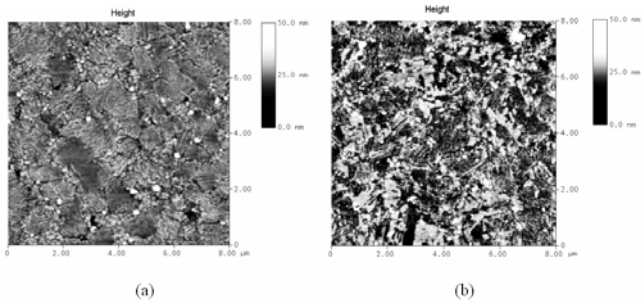

Fig. 13 Topography of 1μm copper thin film by AFM: a) raw thin film; b) shocked film (scanning area 8μm×8μm, data scale 2μm)

Table 1: Microstructure changes of 1μm copper thin film after LSP

Area percentage	Before μLSP	After μLSP
stress-free	57.8%	42.6%
with substructure	24.7%	29.5%
Highly deformed	17.5%	27.9%

Besides using EBSD to investigate grain structure and crystallographic orientation, subgrain structures can also be quantitatively analyzed through EBSD measurements because of its high spatial and angular resolution, such as ~25nm and ~0.8° for the W-filament SEM, respectively. The thinner lines in Fig. 11(a) and (b) show the subgrain boundaries, whose misorientation angles are larger than 1°, of the 1μm copper film without and with LSP, respectively. The red area stands for highly deformed grains, which have the highest density of substructures such as twins and dislocations; the silver area stands for grains with substantial substructures, and the white area is the stress free grains that have less defects and substructures. Compared these two maps, it is observed that there is a great increase in substructure and in highly deformed region after LSP. Table 1 summarizes such changes.

The substructures change due to LSP is featured by high speed and high uniformity compared with normal deformation processes such as cold rolling. Shock front serves as subgrain structure (dislocation) sources when the shock pressure is higher than the critical shear stress. It can be found that most of highly deformed regions (Fig. 11b) are corresponding to (001) texture component as shown in Fig. 14, indicated by corresponding circles. This is likely due to the following two reasons according to properties of anisotropy for individual grains. The first is that the smallest Young's modulus is along <001> direction so that the deformation is easy to occur along <001> direction. The second can be explained by Schmid's law. For FCC crystal, it is well known that the plastic slip systems are the (111) planes in the <110> directions, for a total of 12 possible slip systems. For the (111) orientation grains, there are 6 possible activated slip systems with Schmid's factor -0.272. For the (001) orientation, there are 8 possible activated slip systems with Schmid's factor ±0.408. As a result, it is more difficult to deform in the (111) orientation compared with the (001) orientation.

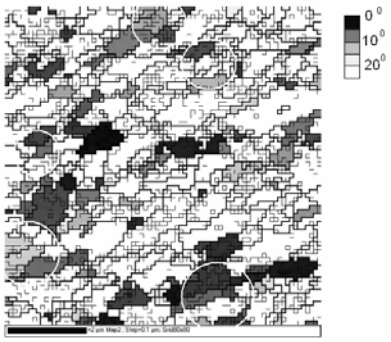

Fig. 14 (001) texture component corresponding to Fig. 11(b), the darker, the closer to the <001> direction; white regions are greater than 20 degrees

The substantial increase of substructures is the major cause of strength and hardness improvement in LSP. With the increase of substructures, the subgrain size decreases, which has an effect similar to grain refinement. As a result, the yield strength of copper thin film increases after LSP. Both the compressive surface residual stress and the refined microstructure in LSP contribute to the fatigue life improvement.

FEM Simulation For The Silicon Substrate

Simulation Condition

The above results show that, although copper films underwent appreciable plastic deformation under μLSP, the Si substrate understandably deforms very little. It is probable that the substrate can be treated as a rigid body boundary in modeling μLSP of thin films.

To provide further evidence, the (004) Si substrate is numerically modeled and analyzed by assuming shock is applied directly on the substrate. The simulation is based on the theory of single crystal plasticity to be briefly explained in the following paragraph. Although Si has a diamond structure, it is assumed that silicon has a similar deformation mechanism as FCC metals for the following reasons [11]: 1) Diamond structure is similar to the FCC structure. The major difference is that diamond structure has four additional atoms in an unit cell. The (111) plane of a diamond structure is the most dense plane just like FCC metals and expected to slip similarly as FCC metals. 2) Its plastic behaviour is reportedly similar to FCC metals though it can only deform slightly at room temperature.

Based on the theory of single crystal plasticity, a user-material subroutine termed UMAT for single crystal plasticity by Kysar (1997) is incorporated into the finite element program ABAQUS. Crystal shear stress of 1GPa on each slip system is assumed [11]. The temporal dependent shock pressure was modeled by using mass, momentum and energy conservation in axial direction and solved numerically by using Matlab [3]. The pressure was then extended to a non-uniform shock profile with a Gaussian spatial distribution [3] since the beam spot size is relatively small and applied as the loading of the subsequent FEM analysis for the substrate. Simulation was carried out assuming finite geometry. The bottom surface is fixed in position, while all the other side surfaces are set traction free.

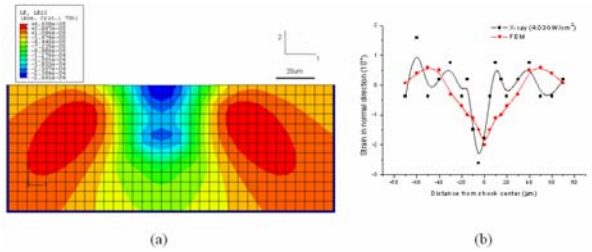

Fig. 15 Strain normal to the irradiated top surface for single crystal silicon: a) strain distribution by FEM; and b) comparison between FEM and X-ray results

The induced deformation state is two-dimensional, i.e., a plane stress deformation state [2] and this point has been explained early in the paper as well. Also, strain rate and hardening effects are ignored in simulation due to the absence of constitutive data in this region. By using this simplified simulation model, the goal is to understand the overall character of the induced deformation and see how much can be predicted. Furthermore, it is hoped that these simulations will lay the ground work for more realistic simulations of thin film with substrate.

Simulation Results And Discussion

Fig. 15(a) shows the contour of strain distribution in normal direction for laser energy 4.03GW/cm ^{2}. In order to compare to the result from x-ray measurement, the in-depth strain is averaged over the effective penetration distance of x-ray. Considering 90 percent absorption, the effective penetration depth can be calculated and is about 42μm [5]. By averaging strains in depth of 42μm, we can find the strain component in normal direction, which is comparable with the result from x-ray (Fig. 15b).

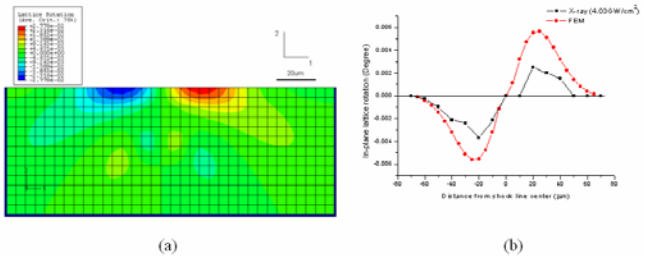

Fig. 16 In-plane lattice rotation for single crystal silicon: a) lattice rotation distribution by FEM; and b) comparison of FEM and X-ray results

Fig. 16(a) shows the contour of the lattice rotation field of the (004) silicon substrate from simulation. Averaging the lattice rotation in Fig. 16(a) in the depth of x-ray penetration, we can compare the simulation result to that of x-ray measurement as shown in Fig. 16(b). They show a similar trend but the FEM result is larger than that from x-ray. It perhaps is due to the fact that the diamond structure of Si is approximated by FCC in FEM and the latter is easier to deform.

Single crystal silicon deforms plastically in an anisotropic manner. In this case, the deformation occurs by the creation and motion of dislocation within the crystal on discrete slip systems under the assumption of plane strain conditions. It is then of interest to study plastic slips in each activated slip system which satisfies this assumption. According to [2], there are three pairs of effective slip systems that satisfy this assumption if a line loading is in the direction of <110> direction as shown in Fig. 17. There are slip system *i*, combination of slip systems $(1\bar{1}1)[011]$ and $(1\bar{1}1)[10\bar{1}]$, slip system *ii*, combination of slip systems $(\bar{1}11)[101]$ and $(\bar{1}11)[0\bar{1}1]$, and complex slip system *iii*, combination of slip systems $(111)[\bar{1}10]$ and $(11\bar{1})[\bar{1}10]$. When activated in equal amounts, the

corresponding two slip systems can combine to form an effective slip system as just mentioned, which act in the (110) plane. Thus, the shock loading generates a predominately plane deformation state in (110) plane if shocking is along [110] direction.

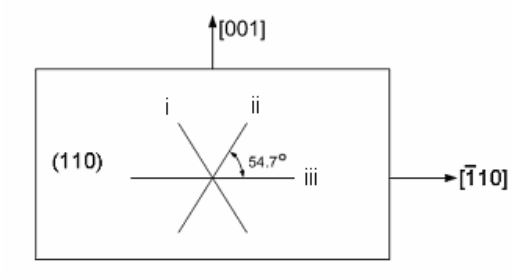

Fig. 17 plane strain slip systems for (001) single crystal sample

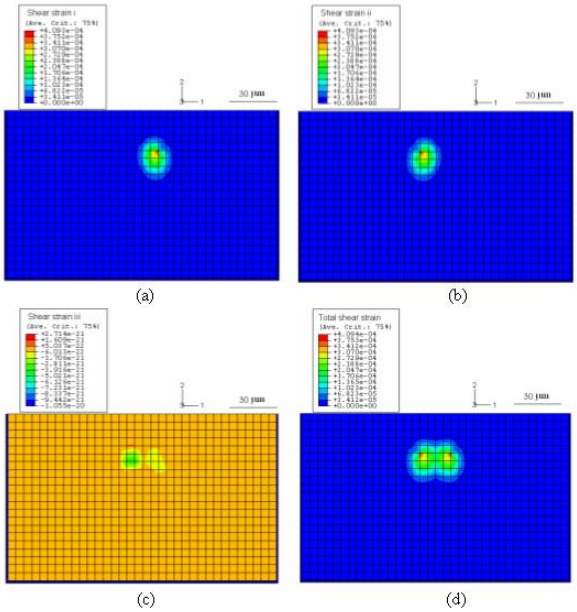

Fig. 18 a) Plastic shear strain for slip system *i*; (b) plastic shear strain for slip system *ii*; (d) plastic shear strain for slip system *iii*; (d) total plastic shear strain (total simulation region is 800μm×400μm)

Fig. 18(a-d) shows the predicted plastic shear strain on each slip system, as well as total accumulated plastic shear strain summed over all slip systems. From Fig. 18(a-b), slip systems *i* and *ii* have the same shear strain distribution because of symmetry. Shear strain in slip system *iii* shown in Fig. 18(c) is much smaller than others because its Schmid's factor is zero. It can be seen that the total shear strain is the vector sum of the shear strains of the three slip systems, which means other slip systems are not activated and is in accordance with the assumption of plane strain deformation. As seen, the slip systems *i* and *ii* are active from a distance to the surface, which can be explained by the distribution of the corresponding resolved shear stress in each slip system. According to Mohr's circle, the contour of resolved shear stress in slip system *i* and *ii* are calculated and shown in Fig. 19. It is seen that the plastic shear strain region (Fig. 18a and b) matches with that of the maximum resolved shear stress in the corresponding slip system (Figs. 19a and b). The maximum resolved shear stress is about 1.051GPa, just above the critical shear stress of 1GPa set for the simulation. In summary, little plastic deformation was induced by μLSP as evidenced here again in Figs. 18a and b. The maximal shear strain is only 0.04% and thus the Si substrate may be treated as rigid body as far as μLSP applied to thin films is concerned.

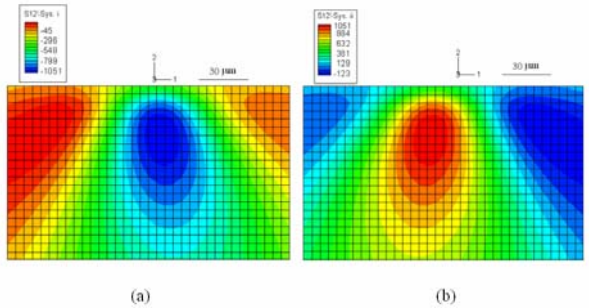

Fig. 19 Resolved shear stress contour in: a) slip system *i*; b)slip system *ii* (corresponding to Fig. 18a and b, respectively, unit is MPa)

Conclusions

In this paper, shock peened copper thin films on (004) single silicon substrate were characterized using micro-diffraction X-ray and EBSD. The induced strain deviation of ±0.025 and dislocation density of 0.7×10^{15} m^{-2} strongly indicate that the non-uniform plastic deformation is induced by μLSP as in bulk metals. Also, microstructure of 1μm films after μLSP was quantified by using EBSD. It was seen that the strong texture (111) was compromised by (001) texture, which can be well understood through the SERM model. In addition, the distribution of grain size after μLSP becomes more uniform and smaller, shown by the results from x-ray diffraction, AFM and EBSD measurements. Both the above trends result in the increase of yield strength of shock peened area, as well as hardness. Besides that, EBSD measurement also shows the increase of subgrain structures that was quantified and used to help explain the fatigue performance improvement by μLSP. To shed some light on the role of the silicon substrate, it was investigated experimentally and via simulation. From

experimental results of the diffraction intensity contrast, strain distribution and lattice rotation, it is clear that the silicon substrate experiences little plastic deformation compared with that of metal films, which is in a good agreement with the results from the FEM simulation. The results were further explored and explained in terms of plastic shear strain and corresponding stress in active slip systems. It appears that the Si substrate can be treated as a rigid body boundary as far as μLSP on thin films is concerned.

Acknowledgement

Support from the National Science Foundation under grant DMI-02-00334 is greatly acknowledged. Dr. Jean Jordan-Sweet of IBM Watson Research Center provided valuable assistance for X-ray micro-diffraction measurements. Assistance in technical details for EBSD provided by Mr. Paul Van Der Wilt is also acknowledged.

References

[1] Spengen, W. M. (2003) MEMS Reliability from a Failure Mechanisms Perspective, Microelectronics Reliability 43, 1049-1060.

[2] Chen, H. Q., Kysar, J. W. and Yao, Y. L. (2003) Characterization of Plastic Deformation Induced by Micro Scale Laser Shock Peening, ASME Journal of Applied Mechanics, submitted.

[3] Zhang, W., Yao, Y. L., and Noyan, I. C. (2004a) Microscale Laser Shock Peening of Thin Films, Part 1: Experiment, Modeling and Simulation, ASME Trans. J. of Manufacturing Science and Engineering, 126, 10-17.

[4] Zhang, W., Yao, Y. L., and Noyan, I. C. (2004b) Microscale Laser Shock Peening of Thin Films, Part 2: High Spatial Resolution Material Characterization, ASME Trans. J. of Manufacturing Science and Engineering 126, 18-24.

[5] Cullity, B. D. (1978) Elements of X-ray Diffraction, London, Addison-Wesley Publishing Company, Inc., Second edition, 268-270.

[6] Ungar, T., Borbely, A. (1996) The effect of dislocation contrast on x-ray line broadening: A new approach to line profile analysis, Applied Physics Letter 69, 3173-3175.

[7] Warren, B. E., Averbach, B. L. (1950) The Effect of Cold-Work Distortion on X-ray Patterns, Journal of Applied Physics 21, 595-599.

[8] Noyan, I. C., and Cohen, J. B. (1987) Residual Stress-Measurement by Diffraction and Interpretation, New York, Springer-Verlag Inc., 168-175.

[9] Lee, D. N. (2000) Strain Energy Release Maximization Model for Evolution of Recrystallization Textures, International Journal of Mechanical Sciences 42, 1645-1678.

[10] Novikov, V. (1997) Grain Growth and Control of Microstructure and Texture in Polycrystalline Materials, New York, CRC Press, 11pp.

[11] Yoshino, M., Aoki, T., Chandrasekaran, N., Shirakashi, T., and Komanduri, R. (2001) Finite Element Simulation of Plane strain plastic-elastic Indentation on Single-Crystal Silicon**,** International Journal of Mechanical Sciences 43, 313-333.

[12] Kysar, J. W. (1997) Addendum to "A User-Material Subroutine Incorporating Single Crystal Plasticity In the ABAQUS Finite Element Program, Mech Report 178," Division of Engineering and Applied Sciences, Harvard University, Cambridge, MA.

Meet the authors

Youneng Wang is a Ph.D candidate at Columbia University. He received his BS and MS from University of Science and Technology of China and University of Michigan, respectively. His research interests are laser shock peening and laser micromachining.

Hongqiang Chen is a Ph.D candidate at Columbia University. He received his BS (1997) and MS (2000) from University of Science and Technology of China. His research interests are laser shock peening and laser micromachining.

Jeffrey W. Kysar is an Assistant professor at Columbia University. He received his Ph.D. from Harvard University and his research interests are micromechanics of fracture in ductile materials, and multi-scale experiments and modelling of fracture.

Y. Lawrence Yao is a Professor at Columbia University. He received his Ph.D. from the University of Wisconsin-Madison in 1988. He is interested in multidisciplinary research in manufacturing and design, nontraditional manufacturing processes and laser materials processing. He serves on the Board of Directors of LIA.